Engineering optical gradient force from coupled surface plasmon polariton modes in nanoscale plasmonic waveguides*

Jiahui Lu(卢佳慧) and Guanghui Wang(王光辉)†

Guangdong Provincial Key Laboratory of Nanophotonic Functional Materials and Devices, South China Normal University, Guangzhou 510006, *China*

(Received 25 March 2016; revised manuscript received 20 July 2016; published online 28 September 2016)

We explore the dispersion properties and optical gradient forces from mutual coupling of surface plasmon polariton (SPP) modes at two interfaces of nanoscale plasmonic waveguides with hyperbolic metamaterial cladding. With Maxwell's equations and Maxwell stress tensor, we calculate and compare the dispersion relation and optical gradient force for symmetric and antisymmetric SPP modes in two kinds of nanoscale plasmonic waveguides. The numerical results show that the optical gradient force between two coupled hyperbolic metamaterial waveguides can be engineered flexibly by adjusting the waveguide structure parameters. Importantly, an alternative way to boost the optical gradient force is provided through engineering the hyperbolic metamaterial cladding of suitable orientation. These special optical properties will open the door for potential optomechanical applications, such as optical tweezers and actuators.

Keywords: hyperbolic metamaterial, waveguide, dispersion, optical force

PACS: 78.67.Pt, 78.20.–e, 42.70.–a **DOI:** 10.1088/1674-1056/25/11/117804

1. Introduction

Optical gradient force and optical tweezers technology, originating from the gradient of a light field, were first pioneered and demonstrated by Ashkin.[1] With the rapid development of modern technology, such optical gradient forces have been broadly exploited in nanoparticles, biomolecules, nanostructures, etc.[2–4] This is attributed to the fact that they have extensive potential applications in optical tweezers,[1,5] optical trapping and manipulating of nanoscale objects.[2,3]

Recently, optical gradient force in the interaction of light with matter has attracted widespread attention. Although the optical force in nanoscale devices is large enough to trap and transport nanoparticles, larger forces would be favorable for experiments. Now, the optical gradient force can be remarkably improved by several orders of magnitude through utilizing coupled high-Q optical resonators,[6–8] coupled optical waveguides,[9,10] and electromagnetic metamaterials.[11,12] Electromagnetic metamaterials, artificially composite electromagnetic structures consisting of subwavelength unit cells, are already the most focused areas in physics and engineering at present. Metamaterials have shown many unusual electromagnetic properties, such as negative refraction,[13] ultrahigh-resolution imaging,[14] and so on. This arises because they may possess negative permittivity or/and permeability at a certain frequency band. Recently, the focus of the metamaterial research has shifted towards hyperbolic metamaterials (HMMs) possessing hyperbolic (or indefinite) dispersion properties. The reason is that HMMs may be flexibly designed to exhibit ultrahigh anisotropy, ultrahigh refractive index, and hyperbolic dispersion, which are not available in natural materials. HMMs enable numerous surprising applications which include optical hyperlens,[15] nanoligraphy,[16] storing light,[17] self-induced torque,[18] and light manipulation.[19]

Recently, the optical force from guided modes in HMMWs has also attracted widespread attention.[20–26] However, the optical force from coupled surface plasmon polariton (SPP) modes in HMMWs is still not clear so far. In this paper, we engineer the dispersion property and optical gradient force for SPP modes in two kinds of nanoscale plasmonic waveguides with hyperbolic metamaterial cladding of different orientations, and provide an alternative way to boost the optical gradient force, which can be remarkably enhanced by designing the hyperbolic metamaterial cladding of suitable orientation and structural parameters.

This paper is structured as follows. In Section 2, we obtain the dispersion relations of SPP modes in two kinds of nanoscale plasmonic waveguides with hyperbolic metamaterial cladding through the Maxwell's equations. In Section 3, according to the Maxwell stress tensor, we derive the compact expression of the optical gradient force from coupled symmetric and antisymmetric SPP modes in the HMMWs. In Section 4, we discuss comparatively the dispersion relation, the effective refractive index, and the average electromagnetic force for symmetric and antisymmetric SPP modes in two nanoscale plasmonic waveguide structures. Finally, a brief summary is given in Section 5.

*Project supported by the National Natural Science Foundation of China (Grant No. 11474106) and the Natural Science Foundation of Guangdong Province, China (Grant No. 2016A030313439).

†Corresponding author. E-mail: wanggh@scnu.edu.cn

© 2016 Chinese Physical Society and IOP Publishing Ltd

2. Dispersion property of SPP modes in HMMWs

We first construct two kinds of nanoscale plasmonic waveguide structures, which are called structure A and structure B in the following. Both of them are made of two semi-infinite HMM layers and a nanoscale slot gap of width d and relative dielectric constant ε_s, as shown in Figs. 1(a) and 1(b). In the two structures (A and B), the HMMs are composed of a period array of metal layer (width a) and germanium layer (width b). It must be emphasized that there is an obvious difference in the two structures. In structure A, the multilayer HMMs are stacked along the x direction. The multilayer HMMs in structure B, however, are stacked along the z direction. As shown in Figs. 1(a) and 1(b), the two semi-infinite HMM layers, respectively, occupy $x > d/2$ and $x < -d/2$ spaces in the Cartesian coordinates. By assuming that the period of the HMMs is much less than the working wavelength, the HMMs can be treated as a homogeneous effective medium, and the effective dielectric permittivity tensor of the HMMs can be modeled as[17,18]

$$\overleftrightarrow{\varepsilon}_{\mathrm{A}} = \varepsilon_0 \begin{pmatrix} \varepsilon_1 & 0 & 0 \\ 0 & \varepsilon_2 & 0 \\ 0 & 0 & \varepsilon_2 \end{pmatrix} \tag{1}$$

in structure A, and

$$\overleftrightarrow{\varepsilon}_{\mathrm{B}} = \varepsilon_0 \begin{pmatrix} \varepsilon_2 & 0 & 0 \\ 0 & \varepsilon_2 & 0 \\ 0 & 0 & \varepsilon_1 \end{pmatrix} \tag{2}$$

in structure B, where $\varepsilon_1 = \varepsilon_{\mathrm{m}}\varepsilon_{\mathrm{d}}/[f_{\mathrm{m}}\varepsilon_{\mathrm{d}} + (1-f_{\mathrm{m}})\varepsilon_{\mathrm{m}}]$ and $\varepsilon_2 = f_{\mathrm{m}}\varepsilon_{\mathrm{m}} + (1-f_{\mathrm{m}})\varepsilon_{\mathrm{d}}$. Here $f_{\mathrm{m}} = a/(a+b)$ is the metal filling ratio in the HMMs, and ε_{d} is the permittivity of the germanium (Ge) in the HMMs. According to the Drude model,[17] the relative permittivity of a metal is $\varepsilon_{\mathrm{m}}(\omega) = \varepsilon_\infty - \omega_{\mathrm{p}}^2/(\omega^2 + \mathrm{i}\omega\gamma)$, where ε_∞ is the background dielectric constant of the metal, ω_{p} is the plasma frequency, and γ is the collision frequency.

We consider a time-harmonic longitudinal SPP mode propagating along the z direction in the three-layer plasmonic waveguide structures, namely, the $\boldsymbol{H}$-field of the SPP mode is only in the y direction, then the $\boldsymbol{H}$-field and the $\boldsymbol{E}$-field can be written as[24]

$$\boldsymbol{H} = \widehat{\boldsymbol{e}}_{\boldsymbol{y}} H_y(x)\, \mathrm{e}^{\mathrm{i}(\beta z - \omega t)}, \tag{3}$$

$$\boldsymbol{E} = [\widehat{\boldsymbol{e}}_{\boldsymbol{x}} E_x(x) + \widehat{\boldsymbol{e}}_{\boldsymbol{z}} E_z(x)]\, \mathrm{e}^{\mathrm{i}(\beta z - \omega t)}, \tag{4}$$

where β is the propagation constant, ω is the angular frequency of the SPP mode, and $\widehat{e}_j$ $(j = x, y, z)$ denotes the unit vector in the j direction.

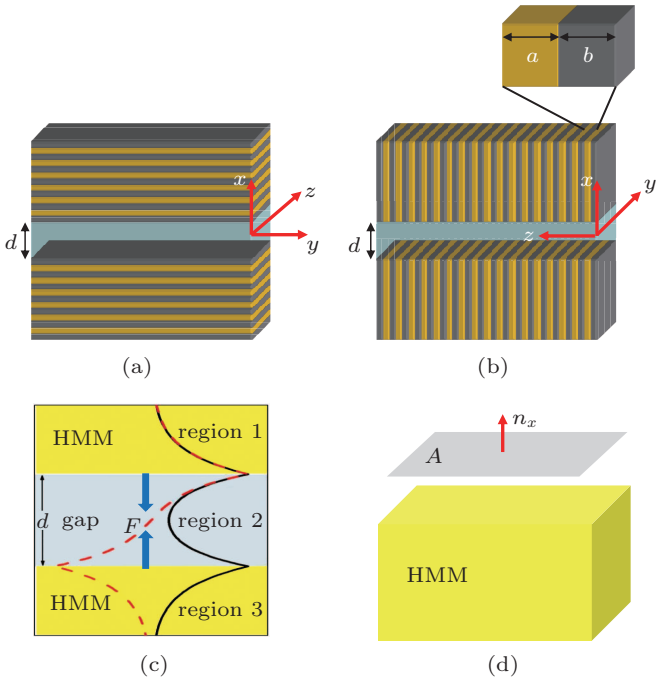


Fig. 1. (color online) Schematic diagram of two nanoscale plasmonic waveguide structures and optical gradient force in such waveguide structures: (a) structure A, (b) structure B. Both structures A and B are constructed by two semi-infinite HMM cladding layers and one nanoscale gap core. The semi-infinite HMMs are composed of alternating insulator (grey) and metal (yellow) thin layers. The coordinate origin is placed at the middle of the gap, and the SPP modes propagate along the z direction. (c) The optical gradient force from mutual coupling of the symmetric SPP mode (black solid line) and the antisymmetric SPP mode (red dashed line). (d) A unit planar surface A parallel to the interface of the waveguide for calculating the optical gradient force.

According to the Maxwell's equations $\nabla \times \boldsymbol{H} = \partial \boldsymbol{D}/\partial t$ and $\nabla \times \boldsymbol{E} = -\mu_0 \partial \boldsymbol{H}/\partial t$, we can obtain the interrelation between the electric field and the magnetic field in the HMM cladding regions $(x > d/2$ and $x < -d/2)$ for structure A as follows:

$$E_x = \frac{\beta}{\varepsilon_0 \varepsilon_1 \omega} H_y, \tag{5}$$

$$\frac{\partial}{\partial x} H_y = -\mathrm{i}\omega\varepsilon_0\varepsilon_2 E_z, \tag{6}$$

$$\frac{\partial}{\partial x} E_z = \mathrm{i}\beta E_x - \mathrm{i}\mu_0 \omega H_y, \tag{7}$$

where ε_0 and μ_0 are the permittivity and permeability of vacuum, respectively. The interrelation between the electric field and the magnetic field in the gap region $(-d/2 < x < d/2)$ can be obtained by changing both ε_1 and ε_2 to ε_s in Eqs. (5)–(7). The general form of $H_y(x)$ for the SPP mode in the three-layer structure A can be expressed as

$$H_y(x) = \begin{cases} H_1\, \mathrm{e}^{-q_{\mathrm{m}}(x-d/2)}, & x > d/2, \\ H_2\, \mathrm{e}^{q_{\mathrm{l}}x} + H_2'\, \mathrm{e}^{-q_{\mathrm{l}}x}, & -d/2 \le x \le d/2, \\ H_3\, \mathrm{e}^{q_{\mathrm{m}}(x+d/2)}, & x < -d/2, \end{cases} \tag{8}$$

where q_{m} and q_{l} are the x-components of the SPP wave vector in the HMM cladding and the dielectric core, respectively; H_1,

H_2, H_2', and H_3 are the amplitudes of the H-field in the different regions, which can be obtained by using the boundary conditions and the initial condition of the field. The continuity boundary conditions of the tangential components of the SPP mode can be expressed as

$$H_{y1}(d/2) = H_{y2}(d/2), \quad H_{y2}(-d/2) = H_{y3}(-d/2), \tag{9}$$

$$E_{z1}(d/2) = E_{z2}(d/2), \quad E_{z2}(-d/2) = E_{z3}(-d/2), \tag{10}$$

where H_{yn} and E_{zn} $(n = 1,2,3)$ denote the tangential magnetic and electric fields in region n, respectively. By inserting Eq. (8) into Eqs. (5)–(7) and the corresponding equations of fields in the gap region $(-d/2 < x < d/2)$, one can obtain

$$q_{\mathrm{m}} = \left(\frac{\varepsilon_2}{\varepsilon_1}\beta^2 - \varepsilon_2\frac{\omega^2}{c^2}\right)^{1/2}, \tag{11}$$

$$q_{\mathrm{l}} = \left(\beta^2 - \varepsilon_{\mathrm{s}}\frac{\omega^2}{c^2}\right)^{1/2}. \tag{12}$$

Note that q_{m} and q_{l} should be real, in other words, $\varepsilon_2\beta^2/\varepsilon_1 - \varepsilon_2\omega^2/c^2 > 0$ and $\beta^2 - \varepsilon_{\mathrm{s}}\omega^2/c^2 > 0$. Then based on the continuous conditions of E_z and H_y at the two interfaces of the three-layer waveguide structure A, we can obtain two different SPP modes in structure A: one, corresponding to $H_2 = H_2'$ and $H_1 = H_3$, is a symmetric SPP mode satisfying the dispersion relation

$$\varepsilon_{\mathrm{s}}q_{\mathrm{m}} + \varepsilon_2 q_{\mathrm{l}}\tanh\left(\frac{q_{\mathrm{l}}d}{2}\right) = 0, \tag{13}$$

the other, corresponding to $H_2 = -H_2'$ and $H_1 = -H_3$, is an antisymmetry SPP mode with the dispersion relation

$$\varepsilon_{\mathrm{s}}q_{\mathrm{m}} + \varepsilon_2 q_{\mathrm{l}}\coth\left(\frac{q_{\mathrm{l}}d}{2}\right) = 0. \tag{14}$$

By the same methods and steps as above, the dispersion relations of the symmetric and antisymmetric SPP modes in structure B can be, respectively, obtained as

$$\varepsilon_{\mathrm{s}}q_{\mathrm{m}}' + \varepsilon_1 q_{\mathrm{l}}'\tanh\left(\frac{q_{\mathrm{l}}'d}{2}\right) = 0, \tag{15}$$

$$\varepsilon_{\mathrm{s}}q_{\mathrm{m}}' + \varepsilon_1 q_{\mathrm{l}}'\coth\left(\frac{q_{\mathrm{l}}'d}{2}\right) = 0, \tag{16}$$

with

$$q_{\mathrm{m}}' = \left(\frac{\varepsilon_1}{\varepsilon_2}\beta^2 - \varepsilon_1\frac{\omega^2}{c^2}\right)^{1/2}, \tag{17}$$

$$q_{\mathrm{l}}' = \left(\beta^2 - \varepsilon_{\mathrm{s}}\frac{\omega^2}{c^2}\right)^{1/2}, \tag{18}$$

where q_{m}' and q_{l}' are the x-components of the SPP wave vector in the HMM cladding and the dielectric core of structure B, respectively. In addition, q_{m}' and q_{l}' should also be real for the SPP modes. Once we have found the dispersion relation and the field form of the SPP modes, we can try to calculate the optical gradient force between the coupled HMMWs, which originates from the mutual coupling of SPP modes at the two interfaces of the three-layer waveguide structure.

3. Optical gradient force between coupled HMMWs

It is well known that when two waveguides get close enough the interaction of the SPP mode at one interface of the waveguide structure with the other, namely, the mutual coupling of the SPP modes, generates an optical gradient force directed perpendicular to the waveguides. Based on the classic electromagnetic theory, the average optical gradient force in the x direction between two coupled HMMWs can be expressed with the Maxwell stress tensor $\overleftrightarrow{\boldsymbol{T}}$ as[19,27]

$$\langle F_x\rangle = \int_{\mathrm{A}} \langle \overleftrightarrow{\boldsymbol{T}}(\boldsymbol{r},t)\rangle \cdot \hat{\boldsymbol{n}}_{\boldsymbol{x}}\,\mathrm{d}a, \tag{19}$$

where

$$\overleftrightarrow{\boldsymbol{T}}(\boldsymbol{r},t) = \varepsilon_{\mathrm{s}}\varepsilon_0\boldsymbol{E}\boldsymbol{E} - \mu_0\boldsymbol{H}\boldsymbol{H} - (\varepsilon_{\mathrm{s}}\varepsilon_0\boldsymbol{E}^2 + \mu_0\boldsymbol{H}^2)\overleftrightarrow{\boldsymbol{I}}/2,$$

here $\overleftrightarrow{\boldsymbol{I}}$ is the identity tensor; $\langle\cdots\rangle$ denotes the time average value at one oscillation period; $\hat{\boldsymbol{n}}_{\boldsymbol{x}}$ is the unit vector perpendicular to the yz plane. It must be emphasized that in Eq. (19) we integrate the Maxwell's stress tensor on a unit planar surface A parallel to the interface of the waveguides, as shown in Fig. 1(d). $\mathrm{d}a$ is an infinitesimal surface element on the planar surface A. With the distribution of the SPP fields, we can write the average optical gradient force as

$$\langle F_x\rangle = \pm\mu_0|H_2|^2\left(1 - \frac{\beta^2c^2}{\varepsilon_{\mathrm{s}}\omega^2}\right), \tag{20}$$

where $\pm$ correspond to the symmetric and antisymmetric SPP modes, respectively. In Section 2, we have found that $\beta^2 - \varepsilon_{\mathrm{s}}\omega^2/c^2 > 0$ for the SPP modes. Therefore, according to Eq. (20), we can easily find that the average electromagnetic force $\langle F_x\rangle$ is always attractive (negative) for the symmetric SPP modes, while it is always repulsive (positive) for the antisymmetric SPP modes. Because of the symmetrical characteristic of the waveguide structure, we can easily show that the optical forces in the y and z directions are equal to zero, namely, $\langle F_y\rangle = 0$ and $\langle F_z\rangle = 0$, due to the reflection symmetry of the whole setup with respect to the xz plane and the xy plane.

In Eq. (20), in order to analyze the optical gradient force, we need to utilize the dispersion relations of the SPP modes and $|H_2|^2$ due to the optical force proportional to the intensity of the fields. Whereas $|H_2|^2$ can be obtained by the total energy flux distribution. The total energy flux per unit length in the z direction can be defined as[28–30]

$$P_z = \int\int_{-\infty}^{+\infty} \langle \boldsymbol{S}\rangle \cdot \hat{\boldsymbol{e}}_{\boldsymbol{z}}\,\mathrm{d}x\mathrm{d}y$$

$$= \frac{1}{2}\int\int_{-\infty}^{+\infty} \mathrm{Re}[\boldsymbol{E}\times\boldsymbol{H}^*]\cdot\hat{\boldsymbol{e}}_{\boldsymbol{z}}\,\mathrm{d}x\mathrm{d}y, \tag{21}$$

where $\boldsymbol{S}$ denotes the Poynting vector, and $*$ denotes the complex conjugate. By inserting Eqs. (3) and (4) into Eq. (21), we can derive the expression of the total energy flux per unit length

$$P = \frac{p_z}{W} = \int_{-\infty}^{+\infty} \frac{\beta}{2\omega\varepsilon}|H_y|^2\,\mathrm{d}x, \tag{22}$$

where W denotes the waveguide width in the y direction, and ε is the corresponding dielectric permittivity of each layer in the plasmonic waveguide of the three-layer structures.

Choosing structure A as an example, we can obtain the interrelation between P and $|H_2|^2$ as follows:

$$P = \frac{|H_2|^2\beta}{2\omega\varepsilon_0}\left[\frac{\mathrm{e}^{q_1 d}-\mathrm{e}^{-q_1 d}}{q_1\varepsilon_\mathrm{s}} \pm \frac{2d}{\varepsilon_\mathrm{s}} + \frac{(\mathrm{e}^{q_1 d/2}\pm\mathrm{e}^{-q_1 d/2})^2}{q_\mathrm{m}\varepsilon_1}\right], \tag{23}$$

where $\pm$ correspond to the symmetric and antisymmetric SPP modes, respectively. By inserting Eq. (23) into Eq. (20), we can derive the expression of the average optical gradient force in the x direction

$$\langle F_x\rangle = \pm\mu_0 P\left(1-\frac{\beta^2c^2}{\varepsilon_\mathrm{s}\omega^2}\right) \times\left\{\frac{\beta}{2\omega\varepsilon_0}\left[\frac{\mathrm{e}^{q_1 d}-\mathrm{e}^{-q_1 d}}{q_1\varepsilon_\mathrm{s}} \pm \frac{2d}{\varepsilon_\mathrm{s}} + \frac{(\mathrm{e}^{q_1 d/2}\pm\mathrm{e}^{-q_1 d/2})^2}{q_\mathrm{m}\varepsilon_1}\right]\right\}^{-1}, \tag{24}$$

where $\pm$ correspond to the symmetric and antisymmetric SPP modes, respectively.

For structure B, the average optical gradient force $\langle F_x\rangle$ can be easily obtained through substituting ε_1 with ε_2 in the denominator of the last term in Eq. (24) firstly, and then replacing q_m and q_1 with q'_m and q'_1, respectively.

4. Results and discussion

In the following analysis and discussion, without loss of generality, we choose some parameters, as follows: $\varepsilon_\mathrm{s}=1$ for the gap dielectric core; $\varepsilon_\mathrm{d}=16$ for the dielectric Ge, and the metal is assumed to be gold (Au) with the background dielectric constant $\varepsilon_\infty=5$, the plasma frequency $\omega_\mathrm{p}=1.37\times10^{16}$ rad/s, and the damping coefficient $\gamma=3.68\times10^{13}$ rad/s. The energy flux per unit length $P=1$ mW/μm. According to the dispersion relation of the coupled SPP modes in the three-layer HMMWs, we plot the dispersion curves and the effective refractive indexes in the z direction for the two different HMMW structures (A and B) with $f_\mathrm{m}=0.5$ in Fig. 2. In Fig. 2, the red and blue lines correspond to the symmetric and antisymmetric SPP modes, respectively.

The three dashed lines (I), (II), and (III) are three auxiliary lines. The dispersion curves for the SPP modes in the two different HMMW structures are distributed inside the area that is surrounded by the three auxiliary lines. This happens because the SPP modes in structure A must satisfy the conditions of $\beta^2-\varepsilon_\mathrm{s}(\omega^2/c^2)>0$ and $(\varepsilon_2/\varepsilon_1)\beta^2-\varepsilon_2(\omega^2/c^2)>0$;

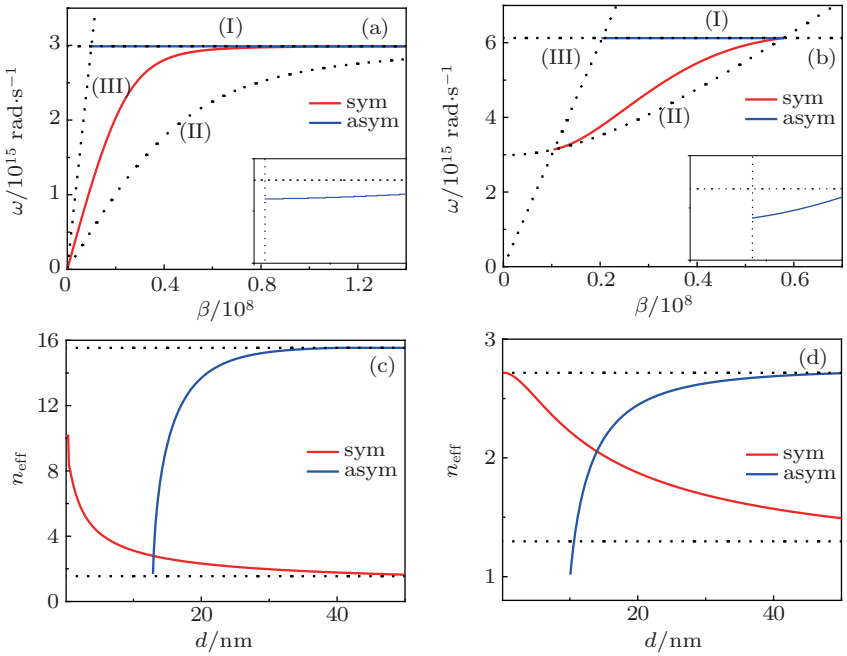


Fig. 2. (color online) Dispersion curves and effective refractive indexes of symmetric (red lines) and antisymmetric (blue lines) modes with $d=10$ nm. Panels (a) and (b) show the dispersion curves of SPP modes in structures A and B, respectively. The insets show the dispersion curves of the antisymmetric SPP modes by amplifying the longitudinal-coordinate axis. (c) The effective refractive index of symmetric mode with $\omega=2.5\times10^{15}$ rad/s and asymmetric mode with $\omega=2.989\times10^{15}$ rad/s in structure A. (d) The effective refractive index of symmetric mode with $\omega=5.5\times10^{15}$ rad/s and asymmetric mode with $\omega=6.124\times10^{15}$ rad/s in structure B.

similarly, the SPP modes in structure B must satisfy the conditions of $\beta^2 - \varepsilon_s(\omega^2/c^2) > 0$ and $(\varepsilon_1/\varepsilon_2)\beta^2 - \varepsilon_1(\omega^2/c^2) > 0$. From Fig. 2, we can see that all of the dispersion curves increase monotonously with the increase of angular frequency ω. The dispersion curve of the antisymmetric modes and curve (I) seem to be coincident but if the longitudinal-coordinate axis is amplified, as shown in the insets of Figs. 2(a) and 2(b), then we can see that the antisymmetric mode curve is also in the region surrounded by the three auxiliary lines. From Figs. 2(a) and 2(b), we can see some obvious difference of the dispersion curves between the two different waveguide structures. In structure A, the dispersion curves of both symmetric and antisymmetric modes asymptotically trend towards a limiting value, $\omega_L = 2.989 \times 10^{15}$ rad/s, in the large β region. In the small β region, the symmetric mode does not have a cut-off frequency, while the antisymmetric mode has a cut-off frequency ω_c, the intersection point between the blue line and line (III). In structure B, whether in the large β region or the small β region, the dispersion curves of both symmetric and antisymmetric modes are cut off. These characteristics of the dispersion curves would directly influence the refractive indexes.

We plot the effective refractive index ($n_{eff} = c\beta/\omega$) in the z direction as a function of gap width d in Figs. 2(c) and 2(d), which are corresponding to structures A and B, respectively. As shown in Figs. 2(c) and 2(d), with the increase of gap width d, the effective refractive index for the symmetric SPP mode (red line) decreases gradually, while the effective refractive index for the antisymmetric SPP mode (blue line) increases gradually. It is worth noting that there is an obvious difference between the symmetric SPP mode and the antisymmetric SPP mode. It is that the antisymmetric mode dose not have any solution in the small gap width. In other words, there exist no antisymmetric SPP modes when the gap width is less than a certain critical value. Both the optical force and the effective refractive index have the same cut-off region. It is not hard to find that the effective refractive index of the SPP modes in structure A is significantly higher than that in structure B. These characteristics of the dispersion and the effective refractive index for the SPP modes in the two types of HMMWs would importantly influence the optical gradient force.

We will next discuss the average electromagnetic force for the symmetric and antisymmetric SPP modes in the two different waveguide structures according to expression (24). As shown in Fig. 3, we plot the optical gradient force $\langle F_x \rangle$ as a function of gap width d for three different filling ratios $f_m = 0.5$, 0.6, and 0.7, which are illustrated by the black solid, red dashed, and blue dotted lines, respectively. From Fig. 3, we can see that the average optical gradient force $\langle F_x \rangle$ is always negative (attractive force) for the symmetric SPP modes, while it is always positive (repulsive force) for the antisymmetric SPP modes. Moreover, in structure A, the optical attractive force for the symmetric SPP modes first decreases rapidly and then relaxedly decreases with the gap width d increasing, as shown in Fig. 3(a). This is because the SPP coupling between the two surface modes at the interfaces becomes weaker and weaker with the increase of the gap width, leading to the optical attractive force between the two surface modes weakened gradually. In Fig. 3(b), the optical repulsive force for the antisymmetric modes sharply decreases with the increase of the gap width d. Compared with the SPP symmetric modes, there exists a cut-off gap width d_c for the antisymmetric modes. It is not hard to find that the cut-off gap width for $f_m = 0.5$, 0.6, and 0.7 is equal to 13 nm, 42 nm, and 50 nm, respectively. This indicates that f_m directly influences the range of the cut-off region, which can be interpreted physically as follows. In Fig. 2(a), the intersection point of the dispersion curve of the antisymmetric mode (blue line) and dashed line (III) is the cut-off frequency ω_c. By inserting Eq. (14) into $\varepsilon_2\beta^2/\varepsilon_1 - \varepsilon_2\omega^2/c^2 = 0$, we can obtain $\omega_c = c\sqrt{\varepsilon_1\varepsilon_2/(1-\varepsilon_1)}/d$. It is well known that the angular frequency of the SPP antisymmetric modes should satisfy $\omega > \omega_c$, which leads to the condition $d > d_c = c\sqrt{\varepsilon_1\varepsilon_2/(1-\varepsilon_1)}/\omega$ for the SPP antisymmetric modes. The cut-off gap width d_c grows with the increase of f_m, so f_m evidently influences the range of the cut-off region. In Fig. 3(c), the optical attractive force for the symmetric SPP modes first increases sharply and then slowly decreases with the gap width d increasing. In other words, for a suitable gap width, all symmetric modes in structure B have their own maximum optical attractive forces. From Fig. 3(d), we can see that the antisymmetric modes all cut off below the 10 nm region, and f_m has not too much influence on the optical repulsive force for the antisymmetric modes in structure B. From Fig. 3, we can see that the optical forces in structure A would be much larger than those in structure B. We will now explain the physics behind this. Through proper simplification of Eq. (24), the average optical gradient force in structure A can be written as $\langle F_x \rangle = -\mu_0 P(n_{eff}^2 - 1)\{[4d + 4/(q_m\varepsilon_1)]n_{eff}/2\varepsilon_0 c\}^{-1}$ for the symmetric SPP mode, and $\langle F_x \rangle = \mu_0 P(n_{eff}^2 - 1)[n_{eff}q_1^2 d^2/(2\varepsilon_0 c q_m \varepsilon_1)]^{-1}$ for the antisymmetric SPP mode. In structure B, $\langle F_x \rangle = -\mu_0 P(n_{eff}^2 - 1)\{[4d + 4/(q'_m\varepsilon_2)]n_{eff}/2\varepsilon_0 c\}^{-1}$ for the symmetric SPP mode, and $\langle F_x \rangle = \mu_0 P(n_{eff}^2 - 1)[n_{eff}q_1'^2 d^2/(2\varepsilon_0 c q'_m \varepsilon_2)]^{-1}$ for the antisymmetric SPP mode. Because $q_1 d < 1$ in structure A and $q'_1 d < 1$ in structure B, the optical gradient force for the antisymmetric modes is greater than that for the symmetric modes. Furthermore, the optical gradient force for the antisymmetric SPP mode in structure A is greater than that in structure B. This is because the effective refractive index n_{eff} in structure A is larger than that in structure B, as shown in Figs. 2(c) and 2(d). These properties provide more advantages to obtain a much larger optical gradient force for optomechanical applications in optical tweezers and actuators.

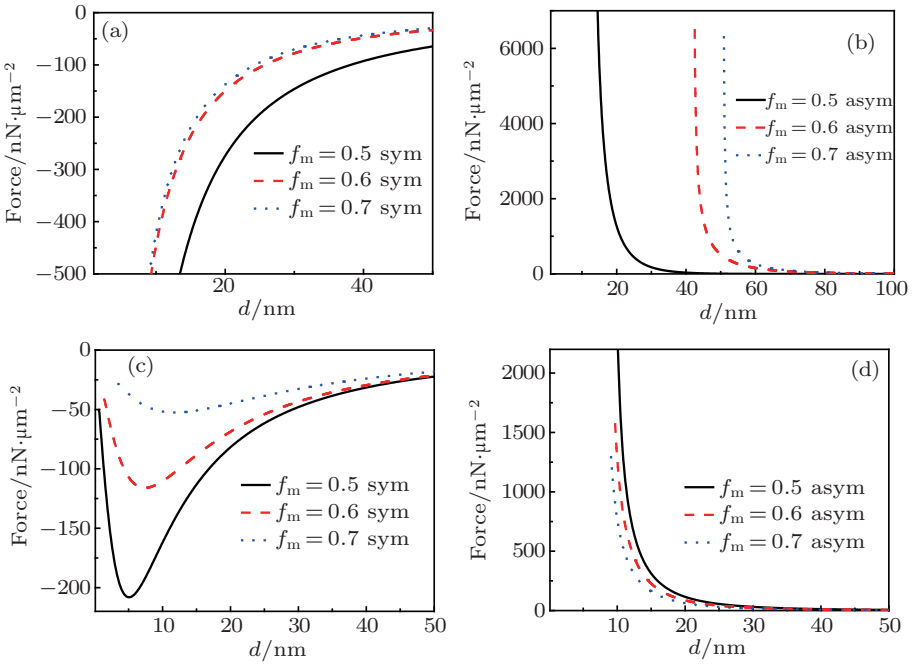


Fig. 3. (color online) Optical gradient force of symmetric and antisymmetric SPP modes as a function of gap width d for different metal filling ratios with $\varepsilon_s = 1$. Panels (a) and (b) are for structure A, (c) and (d) for structure B.

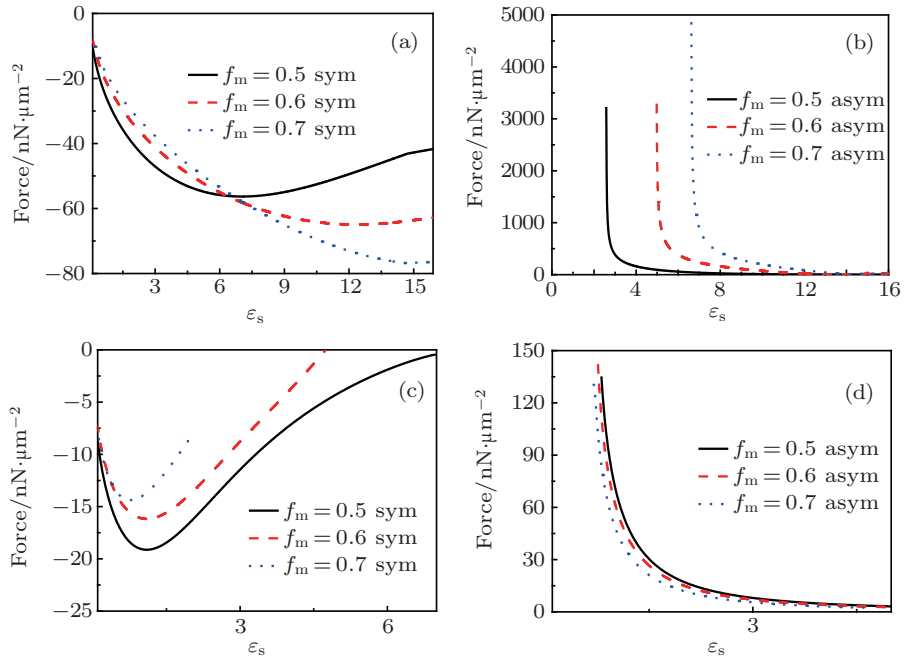


Fig. 4. (color online) Optical gradient force of symmetric and antisymmetric SPP modes versus the relative permittivity ε_s of the gap dielectric for different metal filling ratios with gap width $d = 60$ nm. Panels (a) and (b) are for structure A, (c) and (d) for structure B.

In order to study the influence of the dielectric surrounding on the optical force, we plot the optical gradient force as a function of the permittivity ε_s for different f_m in Figs. 4(a) and 4(c) for the symmetric modes, and in Figs. 4(b) and 4(d) for the antisymmetric modes, with $d = 60$ nm. From Figs. 4(a) and 4(c), we find that the optical attractive force for the symmetric modes firstly increases and then decreases as ε_s increases, and they have different peak values for different f_m. From Figs. 4(b) and 4(d), we can find whether in structure A or structure B, the optical gradient force for the antisymmetric SPP mode always decreases as ε_s increases, and the antisymmetric modes have a cut-off region in the small ε_s region, which depends on the value of f_m. Therefore, we can see that the permittivity ε_s has an important influence on the existence of the SPP modes and the optical force. Under the same conditions, the optical forces in structure A would be much larger than those in structure B. In other words, when the optical force including attractive and repulsive forces in structure B is close to zero, the optical force in structure A is still large enough to carry out experiments in optomechanics. These

properties indicate that the optical gradient force between two coupled plasmonic waveguides may be flexibly engineered to meet various engineering requirements through adjusting the waveguide structure parameters, such as the metal filling ratio, the permittivity of the gap dielectric, and the suitable orientation of the hyperbolic metamaterial cladding. Now, our study shows that the optical gradient force between two coupled hyperbolic metamaterial waveguides can be engineered by the hyperbolic metamaterial cladding of suitable orientation. Based on these advantageous properties of such plasmonic waveguide structures, one can expect that a larger optical gradient force can be applied to optical tweezers and actuators. On the one hand, the larger optical gradient force has advantages to control the growth and self-assembling of artificially synthetic materials, such as electromagnetic metamaterials, photonic crystals, or random sphere assemblies.[31] The larger optical gradient force can be utilized to engineer the mechanical motion of nano-objects and nano-devices, which would be favorable for actuating nanophotonic systems.

5. Summary

We have engineered the optical gradient force in two kinds of nanoscale plasmonic waveguides with hyperbolic metamaterial cladding. By changing the orientation of the hyperbolic metamaterial cladding, different dispersion relations and average electromagnetic forces for symmetric and antisymmetric SPP modes in the coupled nanoscale plasmonic HMMWs can be obtained, and a very large optical gradient force for the coupling SPP modes is shown. In addition, we also demonstrate that the optical gradient force is closely dependent on the metal filling ratio, the dielectric permittivity of the gap core, and the gap width. The designed nanoscale plasmonic waveguide structures provide a more advantageous way to obtain a much larger optical gradient force. These special optical properties will open the door for various optomechanical applications, such as optical tweezers and actuators.

References

[1] Ashkin A 1970 *Phys. Rev. Lett* **24** 156
[2] Sudeep M, Xavier S and David E 2010 *Nano Lett* **10** 99
[3] Yang A H J, Moore S D, Schmidt B S, Matthew K, Michal L and David E 2009 *Nature* **457** 71
[4] Li M, Pernice W H P, Xiong C, Baehr-Jones T, Hochberg M and Tang H X 2010 *Nature* **456** 480
[5] Chu S 1991 *Science* **253** 861
[6] Povinelli M L, Johnson S G, Loncar M, Ibanescu M, Smythe E J, Capasso F and Joannopoulos J D 2005 *Opt. Express* **13** 8286
[7] Matt E, Ryan C, Jasper C, Vahala K J and Oskar P 2009 *Nature* **459** 550
[8] Rakich P T, Popovic M A, Soljacic M and Ippen E P 2007 *Nat. Photon.* **1** 658
[9] Almeida V R, Xu Q, Barrios C A and Lipson M 2004 *Opt. Lett.* **29** 001209
[10] Povinelli M L, Marko L, Mihai I, Smythe E J, Johnson S G, Federico C and Joannopoulos J D 2005 *Opt. Lett.* **30** 003042
[11] Yang X, Liu Y, Oulton R F, Yin X and Zhang X 2011 *Nano Lett.* **11** 321
[12] Yingran H, Sailing H and Yang X D 2012 *Chin. Phys. B* **37** 002907
[13] Jie Y, Zhaowei L, Yongmin L, Yuan W, Cheng S, Guy B, Stacy A M and Zhang X 2008 *Science* **321** 930
[14] Pendry J B 2000 *Phys. Rev. Lett.* **85** 3966
[15] Hyesog L, Zhaowei L, Yi X, Cheng S and Xiang Z 2007 *Opt. Express* **15** 015886
[16] Yan W, Wubs M, Mortensen N A 2012 *Phys. Rev. B* **86** 205429
[17] Lu W T, Huang Y J, Casse B D F, Banyal R K and Sridhar S 2010 *Appl. Phys. Lett.* **96** 211112
[18] Pavel G, Krasavin A V, Poddubny A N, Belov P A, Kivshar Y S and Zayats A V 2013 *Phys. Rev. Lett.* **111** 036804
[19] Yingran H, Sailing H, Jie G and Xiaodong Y 2012 *Opt. Express* **20** 022372
[20] Rho J, Ye Z, Xiong Y, Yin X, Liu Z, Choi H, Bartal G and Zhang X 2010 *Nat. Commun.* **1** 749
[21] Casse B D F, Lu W T, Huang Y J, Gultepe E, Menon L and Sridhar S 2010 *Appl. Phys. Lett.* **96** 023114
[22] Tian J, Junming Z and Yijun F 2009 *Opt. Express* **17** 000170
[23] Wei Y, Asger M N and Martijn W 2013 *Opt. Express* **21**
[24] Boardman A D 1982 *Electromagnetic Surface Modes* (New York: Wiley) pp. 12–14
[25] Valagiannopoulos C A, Mirmoosa M S, Nefedov I S, Tretyakov S A and Simovski C R 2014 *J. Appl. Phys.* **116** 163106
[26] Boardman A D, Egan P and McCall M 2015 *EPJ Appl. Metamat.* **2** 11
[27] Riboli F, Recati A, Antezza M and Carusotto I 2007 *Eur. Phys. J. D* **46** 157
[28] Narimanov E E 2013 *Nat. Photon.* **7** 948
[29] David W, Marko L and Federico C 2009 *Opt. Express* **17** 019996
[30] Zhang W F and Wang G H 2014 *Plasmonics* **9** 979
[31] Riboli F, Recati A, Antezza M and Carusotto I 2007 *Eur. Phys. J. D* **46** 157